Kinetic Simulations of Neoclassical and Anomalous Transport Processes in Helical Systems*)

Hideo SUGAMA[1,2], Tomohiko WATANABE[1,2], Masanori NUNAMI[1,2], Shinsuke SATAKE[1,2], Seikichi MATSUOKA[1] and Kenji TANAKA[1]

[1]*National Institute for Fusion Science, Toki 509-5292, Japan*
[2]*The Graduate University for Advanced Studies (SOKENDAI), Toki 509-5292, Japan*

(Received 10 January 2011 / Accepted 18 May 2012)

Drift kinetic and gyrokinetic theories and simulations are powerful means for quantitative predictions of neoclassical and anomalous transport fluxes in helical systems such as the Large Helical Device (LHD). The δf Monte Carlo particle simulation code, FORTEC-3D, is used to predict radial profiles of the neoclassical particle and heat transport fluxes and the radial electric field in helical systems. The radial electric field profiles in the LHD plasmas are calculated from the ambipolarity condition for the neoclassical particle fluxes obtained by the global simulations using the FORTEC-3D code, in which effects of ion or electron finite orbit widths are included. Gyrokinetic Vlasov simulations using the GKV code verify the theoretical prediction that the neoclassical optimization of helical magnetic configuration enhances the zonal flow generation which leads to the reduction of the turbulent heat diffusivity χ_i due to the ion temperature gradient (ITG) turbulence. Comparisons between results for the high ion temperature LHD experiment and the gyrokinetic simulations using the GKV-X code show that the χ_i profile and the poloidal wave number spectrum of the density fluctuation obtained from the simulations are in reasonable agreements with the experimental results. It is predicted theoretically and confirmed by the linear GKV simulations that the $\boldsymbol{E} \times \boldsymbol{B}$ rotation due to the background radial electric field E_r can enhance the zonal-flow response to a given source. Thus, in helical systems, the turbulent transport is linked to the neoclassical transport through E_r which is determined from the ambipolar condition for neoclassical particle fluxes and influences the zonal flow generation leading to reduction of the turbulent transport. In order to investigate the E_r effect on the regulation of the turbulent transport by the zonal flow generation, the flux-tube bundle model is proposed as a new method for multiscale gyrokinetic simulations.

Keywords: neoclassical transport, anomalous transport, ITG turbulence, zonal flow, gyrokinetic simulation, helical system, LHD

DOI: 10.1585/pfr.7.2403094

1. Introduction

Quantitative predictions of transport fluxes of particles, momentum, and heat in magnetically confined plasmas are a critical issue for the design of fusion reactors. In high-temperature fusion plasmas, where particle mean free paths are much larger than system sizes, kinetic effects such as particle orbits, finite gyroradii, and Landau damping need to be taken into account for accurate analyses of plasma transport processes. These effects can be properly described by kinetic model which treats particle distribution functions on phase space. However, kinetic model is generally more complicated to use than fluid model because the phase-space dimension is higher than the real-space dimension. Therefore, a large number of kinetic transport studies are done by with the help of large-scale computer simulation [1, 2].

In magnetically confined plasmas, there exist collisional and anomalous (or turbulent) transport processes. In the presence of plasma density and temperature gradients, the particle distribution function F deviates from the local Maxwellian f_M and is written as

$$F = f_M + f_1 + \hat{f}_1, \tag{1}$$

where f_1 and $\hat{f}_1$ represent the quasisteady and fluctuating parts of the perturbed distribution function [3]. Using the gyroradius ρ and the equilibrium gradient scale length L, the magnitudes of f_1 and $\hat{f}_1$ are scaled as

$$\frac{f_1}{f_M} \sim \frac{\hat{f}_1}{f_M} \sim \frac{\rho}{L}.$$

Charged particles gyrate around the magnetic field and the gyrophase angle can be chosen as one of the phase space coordinates. Then, the quasisteady perturbed distribution function f_1, which is associated with collisional (classical and neoclassical) transport [4], can be divided into the gyrophase-averaged part $\overline{f}_1$ and the gyrophase-dependent

author's e-mail: sugama.hideo@LHD.nifs.ac.jp

*) This article is based on the invited presentation at the 21st International Toki Conference (ITC21).

part $\tilde{f}_1$:

$$f_1 = \overline{f}_1 + \tilde{f}_1.$$

The gyrophase-dependent part $\tilde{f}_1$, which describes the particle gyro-motion, gives the diamagnetic plasma flows and friction forces in the direction perpendicular to the magnetic field, from which classical transport fluxes of particles and heat are derived. The gyrophase-averaged part $\overline{f}_1$ represents the guiding-center distribution function, from which neoclassical transport fluxes are evaluated. The guiding-center distribution function $\overline{f}_1$ is governed by the drift kinetic equation [5]. In addition to the above-mentioned classical and neoclassical transport, anomalous transport results from turbulent fluctuations driven by microinstabilities [6, 7]. Anomalous or turbulent transport fluxes are derived from the fluctuating part $\hat{f}_1$ of the perturbed distribution function, which is determined by solving the gyrokinetic equation [8–10].

Neoclassical and anomalous transport processes are strongly influenced by toroidal magnetic configurations. In helical systems such as stellarators and heliotrons [11], three-dimensional magnetic structures cause complex particle orbits which yield transport mechanisms different from those in tokamaks. In this paper, recent results from kinetic simulation studies of neoclassical and anomalous transport in helical systems are reported. As an interesting feature of helical plasmas, the link between neoclassical and turbulent transport processes arises through the background radial electric field. Because of the nonaxisymmetry, drift kinetic simulations can determine not only neoclassical particle and heat fluxes but also the background radial electric field from the ambipolarity condition for the neoclassical particle fluxes. Then, the radial electric field produces the $\boldsymbol{E} \times \boldsymbol{B}$ rotation of helical-ripple-trapped particles, which influences the zonal flow generation and accordingly the turbulent transport. In order to treat this effect of the $\boldsymbol{E}\times\boldsymbol{B}$ rotation on the turbulent transport, we propose the gyrokinetic simulation using the flux-tube bundle model in the present work.

The rest of this paper is organized as follows. Examples of drift kinetic simulation are presented in Sec. 2, where radial electric field profiles in Large Helical Device (LHD) plasmas [12] are determined from the ambipolarity condition for the neoclassical particle fluxes obtained by using the global drift kinetic simulation code, FORTEC-3D [13, 14]. Section 3 explains simulation studies using gyrokinetic Vlasov simulation codes, GKV [15, 16] and GKV-X [17–19], to investigate ion temperature gradient (ITG) turbulence and zonal flows in LHD plasmas. In Sec. 4, effects of macroscopic radial electric fields on microscopic zonal flows are discussed and flux-tube bundle model is proposed for new multiscale gyrokinetic simulation to verify the enhancement of zonal flow generation and resultant turbulent transport regulation predicted when increasing the radial electric field. Finally, conclusions are given in Sec. 5.

2. Drift Kinetic Simulation of Neoclassical Transport in Helical Systems

Particles in helical systems are categorized into three classes which show different types of orbits [11]. Two classes of them are passing particles and toroidally trapped particles similar to those in tokamaks while a remaining one consists of particles trapped locally within helical ripples. Drift motion of helical-ripple-trapped particles makes dependence of neoclassical transport on the collision frequency ν and the radial electric field E_r very different from that in tokamaks. In the weakly collisional regime, the neoclassical diffusion coefficient induced by helical-ripple-trapped particles [20, 21] is qualitatively expressed by

$$D \sim \sqrt{\epsilon_\mathrm{h}} v_\mathrm{dr}^2 \frac{\nu_\mathrm{eff}}{\nu_\mathrm{eff}^2 + \omega_\mathrm{E\times B}^2} \propto \begin{cases} \nu_\mathrm{eff}^{-1} & (\nu_\mathrm{eff} \gg |\omega_\mathrm{E\times B}|) \\ \nu_\mathrm{eff}/\omega_\mathrm{E\times B}^2 & (\nu_\mathrm{eff} \ll |\omega_\mathrm{E\times B}|) \end{cases}, \tag{2}$$

where $\sqrt{\epsilon_\mathrm{h}}$, v_dr, and $\nu_\mathrm{eff} \sim \nu/\epsilon_\mathrm{h}$ represent the fraction, the averaged radial drift velocity, and the effective collision frequency of helical-ripple-trapped particles, respectively, and $\omega_\mathrm{E\times B} \sim -cE_\mathrm{r}/rB$ denotes the frequency of the $\boldsymbol{E} \times \boldsymbol{B}$ poloidal rotation.

It is well-known that, in tokamaks, the neoclassical transport fluxes of particles are intrinsically ambipolar; the ambipolarity condition is automatically satisfied by the neoclassical particle fluxes for any radial electric field E_r [4, 5]. On the other hand, because of the above-mentioned ripple transport, the ambipolarity of the neoclassical transport fluxes is nontrivial in helical systems and the radial electric field E_r can be determined from the neoclassical ambipolarity condition [11] which is written for a pure plasma consisting of electrons and a single species of ions as

$$\Gamma_\mathrm{e}^\mathrm{ncl}(E_\mathrm{r}) = \Gamma_\mathrm{i}^\mathrm{ncl}(E_\mathrm{r}). \tag{3}$$

Here, the functions $\Gamma_\mathrm{e}^\mathrm{ncl}$ and $\Gamma_\mathrm{i}^\mathrm{ncl}$ of E_r represent the neoclassical particle fluxes of electrons and ions, respectively. It was confirmed that the radial electric fields predicted from the neoclassical ambipolarity condition are in reasonable agreement with experimental results in helical devices [22, 23] even when the particle fluxes themselves are dominated by anomalous transport. This fact is understandable by noting that the turbulent particle fluxes predicted from the gyrokinetic model are intrinsically ambipolar to the leading order in the gyroradius expansion [3] and therefore they do not contribute to the ambipolarity condition for both helical systems and tokamaks.

A neoclassical transport simulation code, FORTEC-3D, has been developed by Satake *et al.*, which is applicable to general three-dimensional configurations [13, 14]. The FORTEC-3D uses the δf Monte Carlo method and gives a global solution of the drift kinetic equation, which is written as

$$\frac{\partial \overline{f}_1}{\partial t} + v_{\parallel}\boldsymbol{b}\cdot\nabla\overline{f}_1 + \boldsymbol{v}_{\rm d}\cdot\nabla\overline{f}_1 + \boldsymbol{v}_{\rm d}\cdot\nabla f_{\rm M} = C(\overline{f}_1), \quad (4)$$

where $\boldsymbol{v}_{\rm d}$ is the guiding-center drift velocity, C is the linearized collision operator, $\overline{f}_1$ represents the perturbed guiding-center distribution function on the five-dimensional phase space, and the phase space coordinates are given by the guiding-center position (r, θ, ζ), the particle energy $E \equiv mv^2/2 + e\Phi$, and the magnetic moment $\mu \equiv mv_{\perp}^2/(2B)$. The third term $\boldsymbol{v}_{\rm d}\cdot\nabla\overline{f}_1$ on the right-hand side of Eq. (4) contains nonlocal effects due to finite orbit widths (FOWs). The radial electric field $E_{\rm r}$ is also calculated by FORTEC-3D solving

$$\frac{1}{4\pi}\left\langle |\nabla r|^2 \left(1 + \frac{c^2}{v_{\rm A}^2}\right)\right\rangle \frac{\partial E_{\rm r}}{\partial t} = e\left(\Gamma_{\rm e}^{\rm ncl} - \Gamma_{\rm i}^{\rm ncl}\right), \quad (5)$$

with the neoclassical particle fluxes obtained by substituting $\overline{f}_1$ into

$$\Gamma^{\rm ncl} = \left\langle \int {\rm d}^3 v\, \overline{f}_1 \boldsymbol{v}_{\rm d}\cdot\nabla r \right\rangle. \quad (6)$$

Figure 1 shows profiles of the radial electric field in the LHD configuration obtained from the global neoclassical transport simulations using FORTEC-3D and from the ambipolarity condition using the local neoclassical transport model. In the simulations for the cases of Fig. 1, the magnetic field strength on the magnetic axis and the central densities and temperatures for electrons and ions are given by $B_0 = 1.65\,{\rm T}$, $n_{\rm e}(0) = n_{\rm i}(0) = 2\times10^{18}\,{\rm m}^{-3}$, and $T_{\rm e}(0) = T_{\rm i}(0) = 1\,{\rm keV}$. Under the conditions considered in Fig. 1, the global simulations are done only for ions while the the local neoclassical transport model is used for electrons, the FOW effect of which is negligibly small. Details of density and temperature profiles used in the simulations are found in Ref. [14]. The major radius of the vacuum magnetic axis position is given by $R_{\rm ax} = 3.7\,{\rm m}$ and $R_{\rm ax} = 3.6\,{\rm m}$ for the cases of top and bottom panels of Fig. 1, respectively. Neoclassical transport is reduced in the inward-shifted magnetic configuration with the vacuum magnetic axis position $R_{\rm ax} = 3.6\,{\rm m}$ than in the case with $R_{\rm ax} = 3.7\,{\rm m}$ because orbits of helical-ripple-trapped particles show larger radial displacements in the latter case. The difference between the global simulation and local model are not evident near the magnetic axis where helical ripples are small. For the radial region $r/a \geq 0.4$, the difference becomes large because of the ion FOW effect especially for the case of $R_{\rm ax} = 3.7\,{\rm m}$, where the orbit widths of ripple-trapped particles are wider than those for $R_{\rm ax} = 3.6\,{\rm m}$. Thus, the FOW effect tends to enhance the magnitude of the radial electric field $E_{\rm r}$ determined by the ambipolarity condition for the neoclassical particle fluxes. However, it is found that the difference between the resultant ambipolar neoclassical particle fluxes from the local model and the FORTEC-3D is not so large as the change in $E_{\rm r}$ (see Fig. 3 in Ref. [14]).

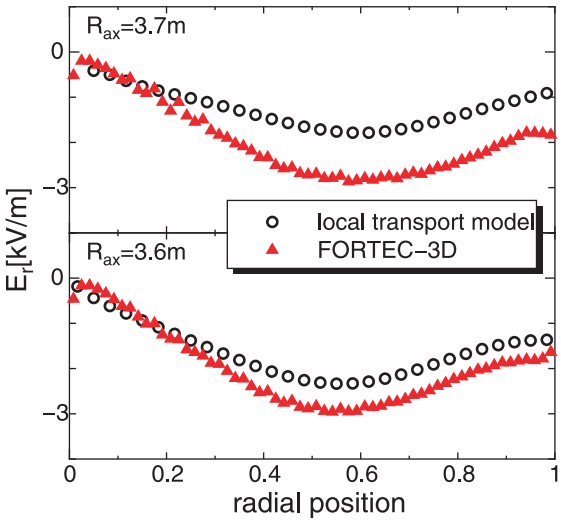

Fig. 1 Profiles of the radial electric field $E_{\rm r}$ in the LHD configuration obtained from the global neoclassical transport simulation using FORTEC-3D (red triangles) and from the ambipolarity condition using the local neoclassical transport model (open circles).

The FORTEC-3D code is also used by Matsuoka *et al*. [24,25] to investigate FOW effects of electron drift motion on the radial electric field formation in Core Electron-Root Confinement (CERC) plasmas [26]. The CERC plasmas obtained in several helical devices are characterized by their high electron temperature ($T_{\rm e}$) and steep $T_{\rm e}$ gradient in the core region, and strong positive radial electric field ($E_{\rm r} > 0$) called the electron root. Comparisons are made between the $E_{\rm r}$ profiles obtained from the FORTEC-3D simulation, the local model, and the experiment for the CERC plasma in LHD. It is confirmed that the difference between the FORTEC-3D simulation and the local model due to the electron FOW effect becomes large in the core region where the steep $T_{\rm e}$ gradient appears. The $E_{\rm r}$ profile obtained from the FORTEC-3D simulation shows a fair agreement with the experimental result except for the edge region where stochastic magnetic fields neglected in the simulation may cause additional electron transport.

As mentioned above, the FOW effect generally enhances the negative $E_{\rm r}$ for high-$T_{\rm i}$ plasmas with $T_{\rm i} \geq T_{\rm e}$ and it also reshapes the strong positive $E_{\rm r}$ profile for CERC plasmas with high $T_{\rm e}$ although, in both cases, the resultant ambipolar neoclassical particle fluxes are found to show smaller changes due to the FOW effect. We also note that, in general, the total transport is dominated by turbulent transport. Thus, the FOW effect is expected to influence the plasma confinement not by changing the neoclassical transport fluxes but by altering $E_{\rm r}$ which can regulate the turbulent transport as discussed in Sec. 4.

3. Gyrokinetic Vlasov Simulation of ITG Turbulent Transport and Zonal Flows in LHD Plasmas

The ITG turbulence is governed by the gyrokinetic equation for the perturbed ion gyrocenter distribution function $\delta f_{\rm i}$,

$$\left[\frac{\partial}{\partial t} + (v_\parallel \boldsymbol{b} + \boldsymbol{v}_{\rm di})\cdot\nabla + \frac{c}{B}(\boldsymbol{b}\times\nabla\overline{\phi})\cdot\nabla\right]\delta f_{\rm i} = (\boldsymbol{v}_{*\rm i} - \boldsymbol{v}_{\rm di} - v_\parallel \boldsymbol{b})\cdot\frac{e\nabla\overline{\phi}}{T_{\rm i}} f_{\rm iM} + C_{\rm i}(\delta f_{\rm i}), \quad (7)$$

and the quasineutrality condition which is represented in the perpendicular wave number vector ($\boldsymbol{k}_\perp$) space as

$$\int {\rm d}^3 v\; J_0(k_\perp v_\perp/\Omega_{\rm i})\delta f_{i\boldsymbol{k}_\perp} - \left[1 - \Gamma_0\left(k_\perp^2\rho_{\rm ti}^2\right)\right]\frac{e\phi_{\boldsymbol{k}_\perp}}{T_{\rm i}} = \frac{e}{T_{\rm e}}\left(\phi_{\boldsymbol{k}_\perp} - \langle\phi_{\boldsymbol{k}_\perp}\rangle\right), \quad (8)$$

where J_0 is the zeroth-order Bessel function and Γ_0 is defined by $\Gamma_0(b) = I_0(b)\exp(-b)$ with the zeroth-order modified Bessel function I_0. The gyrophase-averaged electrostatic potential $\overline{\phi}$ is included in the nonlinear term on the left-hand side of Eq. (7). The right- and left-hand sides of Eq. (8) represent the perturbed ion and electron densities, respectively. Here, for the ITG mode, electrons are assumed to make an adiabatic response to the electrostatic potential. The fluctuation part $\hat{f}_1$ of the particle distribution function in Eq. (1) is given in terms of the perturbed gyrocenter distribution function δf and the potential fluctuation ϕ as

$$\hat{f}_{1\boldsymbol{k}_\perp} = \delta f_{\boldsymbol{k}_\perp}\exp(-i\boldsymbol{k}_\perp\cdot\boldsymbol{\rho}) - \frac{e\phi_{\boldsymbol{k}_\perp}}{T}\left[1 - J_0(k_\perp\rho)\exp(-i\boldsymbol{k}_\perp\cdot\boldsymbol{\rho})\right], \quad (9)$$

where $\boldsymbol{\rho} \equiv \boldsymbol{b}\times\boldsymbol{v}/\Omega$ denotes the gyroradius vector. Simulation studies on ITG turbulence and zonal flows in helical systems are done by using the gyrokinetic Vlasov codes (GKV and GKV-X) which have been developed by Watanabe, Nunami *et al*. [15–19] The GKV and GKV-X codes solve Eqs. (7) and (8) over a toroidal flux-tube domain [27] by using an Eulerian scheme with high phase-space resolution.

It is well-known that turbulent transport can be regulated by zonal flows [15, 28–36] which are generated by turbulent fluctuations themselves. Efficiency of the zonal-flow generation due to the ITG turbulence is described by the response function $\mathcal{K}(t)$. The function $\mathcal{K}(t)$ relates the response of the zonal-flow potential $\phi_k(t)$ at time t to an initially given source $\phi_k(0)$ with $\phi_k(t) = \mathcal{K}(t)\phi_k(0)$, where k is the radial wave number. It is theoretically shown that $\mathcal{K}(t)$ consists of the short- and long-time response parts denoted by $\mathcal{K}_{\rm GAM}(t)$ and $\mathcal{K}_{\rm L}(t)$ [34]. The short-time response part $\mathcal{K}_{\rm GAM}(t)$ represents geodesic acoustic mode (GAM) oscillations [37] which vanishes due to the Landau damping in the long time limit $t \to +\infty$. The long-time response part $\mathcal{K}_{\rm L}(t)$, which shows slow temporal variations, is more important for regulation of turbulent transport than $\mathcal{K}_{\rm GAM}(t)$. For helical systems such as the LHD, the collisionless long-time response function $\mathcal{K}_{\rm L}(t)$ is written as [34]

$$\mathcal{K}_{\rm L}(t) = \frac{1 - (2/\pi)^{1/2}\left\langle(2\epsilon_{\rm H})^{1/2}\{1 - g_{\rm i1}(t,\theta)\}\right\rangle}{1 + G + \mathcal{E}(t)/\left(n_0\langle k_\perp^2\rho_{\rm ti}^2\rangle\right)}, \quad (10)$$

where definitions of $\epsilon_{\rm H}$, $g_{\rm i1}(t,\theta)$, G, and $\mathcal{E}(t)$ are found in Ref. [34] and $\langle\cdots\rangle$ represents the flux-surface average. Equation (10) is derived for long radial wave numbers satisfying $k\rho_{\rm ti} \ll 1$, where $\rho_{\rm ti} \equiv c(m_{\rm i}T_{\rm i})^{1/2}/(eB)$ denotes the thermal ion gyroradius. In the denominator on the right-hand side of Eq. (10), the geometrical factor G is associated with shielding of the zonal-flow potential by toroidally trapped particles while $\mathcal{E}(t)$ represents the shielding effect due to helical-ripple trapped particles. The validity of Eq. (10) is verified by comparison to the linear gyrokinetic simulation for the zonal-flow potential [34].

It is expected from Eq. (10) that zonal-flow generation is enhanced by neoclassical optimization which reduces radial drift of helical-ripple-trapped particles. This theoretical prediction is confirmed by using the GKV code for gyrokinetic simulations of ITG turbulent transport in the helical magnetic fields corresponding to the standard and neoclassically-optimized LHD configurations [15]. For the neoclassically-optimized configuration with an inward-shifted LHD plasma, larger zonal-flow generation and smaller turbulent ion heat transport are obtained by the simulation than for the standard configuration. These theoretical and simulation results are consistent with the LHD experiments [38] which show that not only neoclassical but alsoanomalous transport is reduced in inward-shifted plasmas even though the inward shift increases unfavorable magnetic curvature to destabilize pressure-gradient-driven instabilitiessuch as the ITG mode. Direct comparisons between gyrokinetic simulations and experiments can be made by the GKV-X code [17–19] which uses detailed geometric data of three-dimensional MHD equilibria obtained from the VMEC code [39]. The first validation test of the GKV-X code is done against the high-$T_{\rm i}$ LHD experiment #88343 [40, 41]. Since a $T_{\rm i}$ profile with a steep gradient and a very flattened density profile are observed in this experiment, trapped electron modes (TEMs) are stabilized and turbulent transport is anticipated to be dominantly driven by pure ITG modes which are verified to be considerably unstable in the radial region $0.3 < r/a < 0.9$ by the linear GKV-X simulations [18].

Figure 2 shows turbulent potential structures around $r/a = 0.65$ obtained by the nonlinear GKV-X simulation for the LHD experiment #88343. Three red open symbols in Fig. 3 show the turbulent ion heat diffusivity $\chi_{\rm i}$ at $r/a = 0.46$, 0.65, and 0.83 given by the GKV-X simulations of ITG turbulence under the conditions corresponding to the experiment. Error bars attached to these symbols represent fluctuations of $\chi_{\rm i}$ in the steady-state turbulence

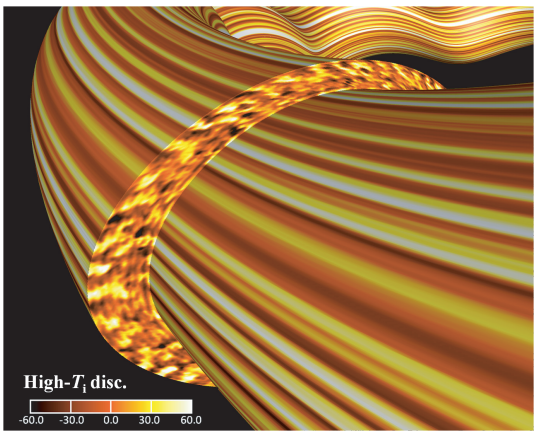

Fig. 2 Turbulent potential structures around $r/a = 0.65$ obtained by the nonlinear GKV-X simulation for in the LHD experiment #88343.

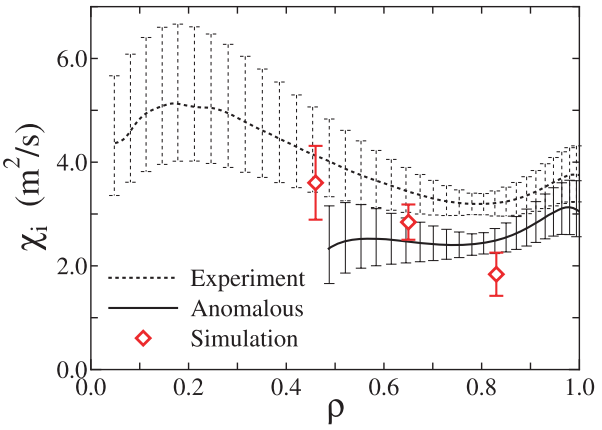

Fig. 3 Radial profiles of the ion heat diffusivities. The solid curve represents the turbulent heat diffusivity obtained by subtracting the neoclassical heat diffusivity from the total heat diffusivity estimated by the LHD experiment #88343 (dotted curve). The red symbols represent the turbulent heat diffusivities at $r/a = 0.46$, 0.65, and 0.83 calculated by the GKV-X simulations.

produced by the simulations. In Fig. 3, a solid curve represents the turbulent heat diffusivity obtained by subtracting the neoclassical heat diffusivity from the total heat diffusivity estimated by the experiment (dotted curve). Error bars for these curves are caused by inaccuracy of the observed ion temperature gradient. We see that the GKV-X simulations reproduce the turbulent ion heat diffusivity χ_i given by the experiment fairly well except that χ_i near the edge ($r/a = 0.83$) is significantly underestimated by the simulation. Plasma beta values at $r/a = 0.46$, 0.65, and 0.83 are roughly given by $\beta \sim 0.4$ %, 0.3 %, and 0.2 %, respectively. For these low beta values, electromagnetic microinstabilities such as kinetic ballooning modes (KBMs) are predicted to be linearly stable while the ITG mode growth rates are expected to be slightly reduced due to electromagnetic effects according to Ref. [42]. Therefore, the present GKV-X simulation results based on the electrostatic model are not considered to be drastically changed by electromagnetic effects although elaborate studies using the electromagnetic model remain as future tasks.

For the LHD experiment #88343, poloidal wave number spectra of the turbulent density fluctuation obtained from the phase contrast imaging (PCI) measurement [43] and from the simulation are compared with each other [19]. The both spectra show similar shapes for high poloidal wave numbers $k_\theta > 0.5\rho_{ti}^{-1}$. The peak position of the spectrum obtained from the experiment is found at a higher poloidal wave number than that obtained from the simulation. However, this quantitative difference appearing in the low poloidal wave number spectra is not conclusive when we take account of a large ambiguity of the experimental results due to the cutoff at $k_\theta \sim 0.4\rho_{ti}^{-1}$ and coarse resolution in the PCI measurement for low poloidal wave numbers. The above-mentioned results showing reasonable agreements between the LHD experiment and simulations encourage us to further gyrokinetic simulation studies for anomalous transport in helical systems.

The GKV-X simulations for the LHD experiment #88343 also show that zonal flows are a critical factor to determine the turbulent ion heat diffusivity χ_i. It is shown from the nonlinear simulation results [19] that χ_i is approximately proportional to $T/Z^{1/2}$ where T and $Z^{1/2}$ represent the square of the turbulent potential amplitude and the mean square root of the zonal-flow potential, respectively, in the saturated turbulence state. As found by M. Nunami *et al.* [19], this relation of χ_i to (T, Z) reflects the fact that, even if the turbulence amplitude T has the same value, the larger zonal flow amplitude Z causes the spectral transfer of turbulent fluctuations into higher radial wave number regions, in which ITG modes are less unstable and turbulent transport occurs inefficiently. We also find that T and Z have significant correlations with the linear ITG growth rate and the linear zonal-flow response. Therefore, it is expected that modeling of χ_i can be done by using results from linear analyses of the unstable modes and zonal flows.

4. Radial Electric Field Effects on Zonal Flows

In the gyrokinetic turbulence simulations explained in the previous section, a local flux-tube domain is used based on the idea of the ballooning representation [44], in which only the neighborhood of a single field line labeled by $\alpha \equiv \theta - \zeta/q(r)$ is considered. For helical systems, the field line label α explicitly appears in the gyrokinetic equation in contrast to tokamak cases although α is regarded as a fixed parameter in the local flux-tube model. However, even if the zonal-flow potential ϕ is independent of α, the explicit appearance of α in the magnetic drift terms of the gyrokinetic equation causes the perturbed gyrocenter distribution function δf to depend on α. Therefore, when tak-

ing account of the equilibrium or macroscopic radial electric field E_r produced by the ambipolarity condition for neoclassical radial particle fluxes (see Sec. 2), the $\boldsymbol{E} \times \boldsymbol{B}$ rotation term, $\omega_{E\times B}\partial\delta f/\partial\alpha$, enters the zonal-flow component of the gyrokinetic equation and influences the zonal-flow response in helical configurations. It is theoretically predicted that $\boldsymbol{E} \times \boldsymbol{B}$ rotation induced by E_r enhances the zonal-flow potential amplitude by reducing radial displacements of helical-ripple-trapped particles [45–48]. When the E_r effect is included, the collisionless long-time response of the zonal-flow potential $\phi_k(t)$ to a initially given source $\phi_k(0)$ is given for $k\rho_{ti} \ll 1$ by [46]

$$\phi_k(t) = \frac{\phi_k(0)}{1 + G_p + G_t + M_p^{-2}(G_{ht} + G_h)(1 + T_e/T_i)}, \tag{11}$$

where geometrical factors G_p, G_t, G_{ht}, and G_h represent shielding effects of neoclassical polarization due to different types of particle orbits existing in helical systems and their definitions are given in Ref. [46]. The radial electric field E_r enters the denominator in the right-hand side of Eq. (11) through the poloidal Mach number defined by $M_p \equiv |(cE_rB_0)/(rv_{ti}/Rq)|$ where q denotes the safety factor. We see from Eq. (11) that zonal-flow generation can be enhanced when the geometrical factors G_{ht} and G_h associated with orbits of helical-ripple-trapped particles are reduced by neoclassical optimization and/or when M_p is increased by increasing E_r or using ions with a heavier mass. Since a higher zonal-flow response is predicted for a heavier ion mass under the identical conditions on the magnitude of E_r and the magnetic geometry, the turbulent transport is expected to show a more favorable ion-mass dependence than the conventional gyro-Bohm scaling [46]. In order to investigate the E_r effect, the simulation domain needs to be extended in the α-direction from the flux tube to the shell region covering the whole magnetic flux surface. Linear gyrokinetic simulations of the zonal-flow response are done by the extended GKV code [49], from which it is confirmed that the linear zonal-flow response is enhanced by increasing E_r as predicted by Eq. (11).

Because of helical ripples, gyrokinetic simulation generally requires higher resolution of the phase space for helical systems than for tokamaks. Especially, nonlinear gyrokinetic simulation for the shell region over the whole flux surface in helical systems needs much more computational memory and time than for a single flux-tube domain. Here, we propose a flux-tube bundle model as a new method for multiscale gyrokinetic simulation which treats the macroscopic $\boldsymbol{E} \times \boldsymbol{B}$ rotation and the microscopic zonal flows with a smaller computational burden than direct simulation for the whole shell region. Based on the scale separation concept, we use the macroscopic (or large scale length) coordinates (r, α, z) and the microscopic (or small scale length) coordinates (x, y). Here, r, $\alpha \equiv \theta - \zeta/q(r)$, and $z \equiv \theta$ represent the radial coordinate, the field-line label, and the poloidal angle, respectively, which are included in the equilibrium (or background) variables; for example, the equilibrium magnetic field strength is written as $B = B(r, \alpha, z)$. The (x, y) coordinates represent the same as (r, α) although (x, y) are used to describe microscopic scale variation of turbulent variables on the plane perpendicular to the magnetic field. For example, the fluctuating potential is written as $\phi = \phi(x, y, z; r, \alpha)$ where (x, y) and (r, α) are treated as independent pairs of coordinates to separately represent microscopic and macroscopic variations.

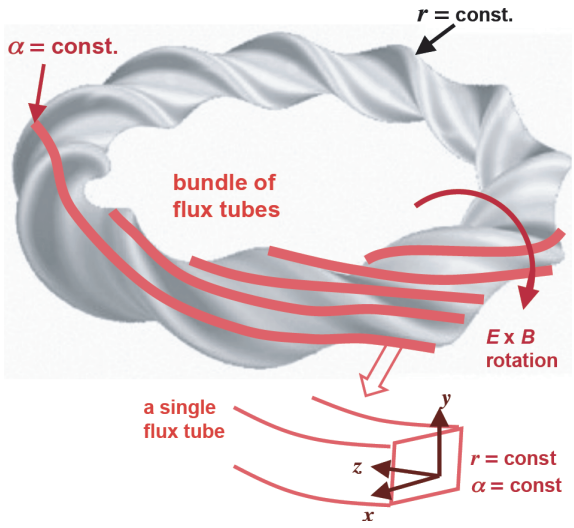

Fig. 4 The flux-tube bundle model. A bundle of flux tubes used for simulation domains are shown in red color.

Figure 4 shows a bundle of flux tubes distributed over a given flux surface labeled by the macroscopic radial coordinate r. Each flux tube is specified by assigning certain constant values to r and α. We note that $z \equiv \theta$ is regarded as the coordinate along the magnetic field line because the direction parallel to the magnetic field is given by changing z with all other coordinates fixed. When microscopic fluctuations are considered for each flux tube, unstable modes such as the ITG instability need to have finite wave numbers $k_y \neq 0$ in the y-direction. For $k_y = 0$, fluctuations give linearly stable modes such as zonal flows. The gyrokinetic equation for the zonal ($k_y = 0$) component of the perturbed ion gyrocenter distribution function $\delta f_i(x, z, E, \mu; r, \alpha)$ is written as

$$\begin{aligned}
&\left[\frac{\partial}{\partial t} + \frac{v_\parallel}{qR}\frac{\partial}{\partial z} + v_{dr}\frac{\partial}{\partial x}\right.\\
&\left.+\omega_{E\times B}\frac{\partial}{\partial \alpha} - C_i\right]\delta f_i(x, z, E, \mu; r, \alpha)\\
&= -\frac{e}{T_i}f_{iM}\left(\frac{v_\parallel}{qR}\frac{\partial}{\partial z} + v_{dr}\frac{\partial}{\partial x}\right)\overline{\phi}(x, z; r, \alpha)\\
&+\mathcal{N}(\overline{\phi}, \delta f_i),
\end{aligned} \tag{12}$$

where $\mathcal{N}(\overline{\phi}, \delta f_i)$ denotes the $k_y = 0$ component of the nonlinear $\boldsymbol{E} \times \boldsymbol{B}$ convection term that is regarded as a source of zonal flows. The effect of the equilibrium ra-

dial electric field E_r on the zonal flow generation appears from the $\boldsymbol{E} \times \boldsymbol{B}$ rotation term $\omega_{E\times B}\partial\delta f_i/\partial\alpha$ on the left-hand side of Eq. (12). This term causes the interaction between the zonal ($k_y = 0$) modes distributed over the bundle of flux tubes with different values of α and thus influences zonal flow generation and turbulent transport. When different flux-tube regions are coupled through the background $\boldsymbol{E} \times \boldsymbol{B}$ rotation in the flux-tube bundle model, the perturbed distribution function is considered to show poloidally-global structures reflecting poloidal excursions of helical-ripple-trapped particles which cannot be grasped by conventional single-flux-tube simulations. We expect from this coupling that the turbulent transport processes are necessarily linked to the neoclassical transport because the ambipolar neoclassical particle fluxes determine the $\boldsymbol{E} \times \boldsymbol{B}$ rotation which can, in turn, enhance zonal-flow generation and accordingly regulate the turbulent transport.

Without the $\boldsymbol{E} \times \boldsymbol{B}$ rotation, turbulent fluctuations in each flux-tube domain are determined independently of those in other flux tubes in the same way as in the case of a single flux tube simulation. In axisymmetric systems such as tokamaks where equilibrium variables do not depend on α, δf_i is set to be independent of α and accordingly the $\boldsymbol{E} \times \boldsymbol{B}$ rotation term has no effect even if $\omega_{E\times B}(\propto E_r) \neq 0$. Gyrokinetic turbulence simulation using the flux-tube bundle model described above is planned to confirm the E_r effect on the zonal flows and the ITG turbulent transport, and its results will be reported elsewhere.

In the LHD experiment #88343, for which the GKV-X simulations are done as described in Sec. 3, the data of the background radial electric field are obtained only near the peripheral region ($r/a \geq 0.8$) (see Fig. 1 in Ref. [18]). The maximum $\boldsymbol{E}\times\boldsymbol{B}$ drift velocity is given from these data by $(v_{E\times B})_{max} \simeq 1.4 \times 10^3$ m/s at $r/a = 0.83$, which corresponds to the poloidal Mach number $M_p \simeq 0.028$. For this small Mach number, the enhancement of the residual zonal flow is anticipated to be weak according to Eq. (11) and Ref. [49]. Thus, as far as the radial electric field is within this level of M_p, we can justify the GKV-X flux-tube simulations in Sec. 3. However, if M_p becomes larger by increasing the radial electric field and/or by using ions with a heavier mass, larger zonal-flow generation and resultant turbulent transport regulation are expected.

It was shown by Anderson and Kishimoto [50] and by Uzawa *et al.* [51] that sheared mean flows can weaken the generation rate of zonal flows by affecting the modulational process. Such an effect of the sheared mean flow on the zonal flow generation is not included in Eqs. (11) and (12) where the background $\boldsymbol{E} \times \boldsymbol{B}$ flow shear is neglected as a smaller term of higher order in ρ/L. The modulational instability analysis of zonal flows including effects of the sheared mean flow in helical systems still remains as one of interesting and complicated subjects.

5. Conclusions

In this paper, recent results from kinetic studies on transport processes in helical systems such as the Large Helical Device (LHD) are reported. These results show that drift kinetic and gyrokinetic theories and simulations are useful tools for quantitative predictions of neoclassical and turbulent transport fluxes with accurate treatment of collective particles' motion in complex three-dimensional magnetic field structures.

In helical systems, ripple-trapped particles give a dominant contribution to neoclassical transport although the ripple transport can be significantly reduced with increasing the radial electric field E_r. In contrast to axisymmetric systems such as tokamaks, E_r profiles in helical systems can be determined by the condition of ambipolar neoclassical radial particle fluxes because of ripple-trapped particles' drift motion causing different dependence of neoclassical transport on the collisionality ν and E_r from that in the axisymmetric case. Using the δf Monte Carlo particle simulation code, FORTEC-3D, which solves the drift kinetic equation in the global toroidal region, radial profiles of the neoclassical particle and heat transport fluxes and the radial electric field in helical systems can be calculated. The FORTEC-3D is used to investigate effects of ion finite orbit widths (FOWs) on the neoclassical transport and the E_r profile in the LHD configurations for the case of equal ion and electron temperatures, where the ion FOW effect are shown to be significant under the conditions corresponding to large radial excursions of ripple-trapped particles. Neoclassical transport simulations using the FORTEC-3D code are also done for Core Electron-Root Confinement (CERC) plasmas with high electron temperature T_e and steep T_e gradient in the core region. Electron FOW effects and a reasonable agreement between the E_r profile obtained from the simulation and the LHD experiment are confirmed for the core region in the CERC plasma.

ITG turbulent transport and zonal flows in helical systems are studied by gyrokinetic Vlasov simulation codes, GKV and GKV-X, which employ a flux tube domain. The GKV simulations show that the turbulent heat diffusivity χ_i is reduced by enhanced zonal flow generation for the neoclassically-optimized magnetic configuration as theoretically predicted. The radial profile of χ_i and the poloidal wave number spectrum of the density fluctuation obtained from the high ion temperature LHD experiment #88343 are compared with the results from the GKV-X simulations which can include precise geometrical data of MHD equilibria corresponding to experiments. The comparisons of the χ_i profiles and the fluctuation spectra show fairly good agreements between the simulations and the experimental results, which imply that we are on the right track toward further studies of anomalous transport in the LHD experiments and future helical reactors based on the gyrokinetic simulations. The GKV-X simulation results also show that χ_i is approximately proportional to the ratio between the

square of the turbulent potential amplitude and the mean square root of the zonal-flow potential in the saturated turbulence state.

It is theoretically predicted that, in helical systems, the macroscopic or background radial electric field E_r can enhance generation of zonal flows leading to the further reduction of turbulent transport and the favorable isotope effect of the ion mass. The enhanced zonal-flow response due to the increased E_r is verified by the linear GKV simulations, for which the simulation domain is extended from the flux tube to the shell region covering the whole magnetic flux surface. In order to confirm the E_r effect on the zonal flows and the ITG turbulent transport, the flux-tube bundle model is proposed as a new method for multiscale gyrokinetic turbulence simulation.

As future tasks, we plan to extend the gyrokinetic simulation codes for including the flux-tube bundle model and other physical processes such as turbulent electron transport and electromagnetic fluctuations.

Acknowledgments

The authors thank Dr. M. Yokoyama and Dr. S. Toda for fruitful discussions on neoclassical transport in helical systems, and also thank the LHD experiment group for providing experimental data and useful discussions on them. This work is supported in part by the Japanese Ministry of Education, Culture, Sports, Science and Technology (Grant Nos. 21560861 and 22760660) and in part by the NIFS Collaborative Research Program (NIFS10KNTT003, NIFS10KNST006, NIFS11KNST017, NIFS11KNXN229, and NIFS11KNST014). Numerical simulations were carried out with the use of the Plasma Simulator and the LHD Numerical Analysis System at the National Institute for Fusion Science.

[1] Y. Idomura, T.-H. Watanabe and H. Sugama, Comptes Rendus Physique **7**, 650 (2006).
[2] X. Garbet, Y. Idomura, L. Villard and T.-H. Watanabe, Nucl. Fusion **50**, 043002 (2010).
[3] H. Sugama, M. Okamoto, W. Horton and M. Wakatani, Phys. Plasmas **3**, 2379 (1996).
[4] P. Helander and D.J. Sigmar, *Collisional Transport in Magnetized Plasmas* (Cambridge University Press, Cambridge, 2002).
[5] S.P. Hirshman and D.J. Sigmar, Nucl. Fusion **21**, 1079 (1981).
[6] W. Horton, Rev. Mod. Phys. **71**, 735 (1999).
[7] W.M. Tang, Nucl. Fusion **18**, 1089 (1978).
[8] A.J. Brizard and T.S. Hahm, Rev. Mod. Phys. **79**, 421 (2007).
[9] E.A. Frieman and L. Chen, Phys. Fluids **25**, 502 (1982).
[10] H. Sugama, Phys. Plasmas **7**, 466 (2000).
[11] M. Wakatani, *Stellarator and Heliotron Devices* (Oxford University Press, Oxford, 1998).
[12] A. Komori, H. Yamada, S. Imagawa *et al*., Fusion Sci. Technol. **58**, 1 (2010).
[13] S. Satake, H. Sugama and T.-H. Watanabe, Nucl. Fusion **47**, 1258 (2007).
[14] S. Satake, M. Okamoto, N. Nakajima, H. Sugama and M. Yokoyama, Plasma Fusion Res. **1**, 002 (2006).
[15] T.-H. Watanabe, H. Sugama and S. Ferrando-Margalet, Phys. Rev. Lett. **100**, 195002 (2008).
[16] T.-H. Watanabe, H. Sugama and S. Ferrando-Margalet, Nucl. Fusion **47**, 1383 (2007).
[17] M. Nunami, T.-H. Watanabe and H. Sugama, Plasma Fusion Res. **5**, 016 (2010).
[18] M. Nunami, T.-H. Watanabe, H. Sugama and K. Tanaka, Plasma Fusion Res. **6**, 1403001 (2011).
[19] M. Nunami, T.-H. Watanabe, H. Sugama and K. Tanaka, Phys. Plasmas **19**, 042504 (2012).
[20] K.C. Shaing, Phys. Fluids **27**, 1567 (1984).
[21] S. Toda and K. Itoh, J. Plasma Fusion Res. **78**, 582 (2002).
[22] M. Yokoyama, A. Wakasa, S. Murakami *et al*., Fusion Sci. Technol. **58**, 269 (2010).
[23] H. Maaßberg, C.D. Beidler, U. Gasparino *et al*., Phys. Plasmas **7**, 295 (2000).
[24] S. Matsuoka, S. Satake, M. Yokoyama, A. Wakasa and S. Murakami, Phys. Plasmas **18**, 032511 (2011).
[25] S. Matsuoka, S. Satake, M. Yokoyama and A. Wakasa, Plasma Fusion Res. **6**, 123016 (2011).
[26] M. Yokoyama, H. Maaßberg, C.D. Beidler *et al*., Nucl. Fusion **47**, 1213 (2007).
[27] M.A. Beer, S.C. Cowley and G.W. Hammet, Phys. Plasmas **2**, 2687 (1995).
[28] A. Hasegawa and M. Wakatani, Phys. Rev. Lett. **59**, 1581 (1987); H. Sugama, M. Wakatani and A. Hasegawa, Phys. Fluids **31**, 1601 (1988).
[29] Z. Lin, T.S. Hahm, W.W. Lee, W.M. Tang and R.B. White, Science **281**, 1835 (1998).
[30] P.H. Diamond, S.-I. Itoh, K. Itoh and T.S. Hahm, Plasma Phys. Control. Fusion **47**, R35 (2005).
[31] K. Itoh, S.-I. Itoh, P.H. Diamond *et al*., Phys. Plasmas 13, 055502 (2006).
[32] A. Fujisawa, K. Itoh, H. Iguchi *et al*., Phys. Rev. Lett. **93**, 165002 (2004).
[33] M.N. Rosenbluth and F.L. Hinton, Phys. Rev. Lett. **80**, 724 (1998).
[34] H. Sugama and T.-H. Watanabe, Phys. Plasmas **13**, 012501 (2006).
[35] P. Helander, A. Mishchenko, R. Kleiber and P. Xanthopoulos, Plasma Phys. Control. Fusion **53**, 054006 (2011).
[36] P. Xanthopoulos, A. Mischchenko, P. Helander, H. Sugama and T.-H. Watanabe, Phys. Rev. Lett. **107**, 245002 (2011).
[37] N. Winsor, J.L. Johnson and J.J. Dawson, Phys. Fluids **11**, 2248 (1968).
[38] H. Yamada, A. Komori, N. Ohyabu *et al*., Plasma Phys. Control. Fusion **43**, A55 (2001).
[39] S.P. Hirshman and O. Betancourt, J. Comput. Phys. **96**, 99 (1991).
[40] K. Ida, M. Yoshinuma, M. Osakabe *et al*., Phys. Plasma **16**, 056111 (2009).
[41] K. Tanaka, C.A. Michael, L.N. Vyacheslavov *et al*., Plasma Fusion Res. **5**, S2053 (2010).
[42] H. Sugama and T.-H. Watanabe, Phys. Plasmas **11**, 3068 (2004).
[43] K. Tanaka, C.A. Michael, L.N. Vyacheslavov *et al*., Rev. Sci. Instrum. **79**, 10E702 (2008).
[44] R.D. Hazeltine and J.D. Meiss, *Plasma Confinement* (Addison-Wesley, Redwood City, 1992) p. 298.
[45] H. Sugama, T.-H. Watanabe and S. Ferrando-Margalet, Plasma Fusion Res. **3**, 41 (2008).
[46] H. Sugama and T.-H. Watanabe, Phys. Plasmas **16**, 056101

(2009).
[47] H. Sugama and T.-H. Watanabe, Control. Plasma Phys. **50**, 571 (2010).
[48] H.E. Mynick and A.H. Boozer, Phys. Plasmas **14**, 072507 (2007).
[49] T.-H. Watanabe and H. Sugama, Nucl. Fusion **51**, 123003 (2011).
[50] J. Anderson and Y. Kishimoto, Phys. Plasmas **13**, 102304 (2006).
[51] K. Uzawa, Y. Kishimoto and J.Q. Li, J. Phys. Soc. Jpn. **77**, 034501 (2008).